Int. J. Appl. Ceram. Technol., 1–7 (2014)
DOI:10.1111/ijac.12319

Additive Manufacturing of Dense Alumina Ceramics

Martin Schwentenwein* and Johannes Homa

Lithoz GmbH, Vienna 1040, Austria

In this study, a new process for additive manufacturing (AM) of dense and strong ceramic objects is described. The lithography-based ceramic manufacturing (LCM) technique is based on the selective curing of a photosensitive slurry by a dynamic mask exposure process. The LCM technique is able to produce strong, dense and accurate alumina ceramics without virtually any geometrical limitations. With over 99.3% of a theoretical alumina density, four-point bending strength of 427 MPa, and very smooth surfaces, the LCM process distinguishes itself from other AM techniques for ceramics and provides parts with very similar mechanical properties as conventionally formed alumina.

Introduction

Additive manufacturing (AM) refers to the production of three-dimensional (3D) structures directly from a computer-aided design (CAD) model in an additive process by the sequential assembly of the individual layers of the object. The concept of employing AM technologies is already state of the art in plastic processing or metalworking;[1] however, the ceramic industry has been reluctant to implement this kind of technology. The reluctance toward this technology was mainly associated with resolution and the quality of the produced parts.[2] Nonetheless, there is a strong need for the introduction of AM technologies for ceramics as conventional manufacturing techniques face a number of limitations. Especially, the production of small-scale series or individual parts such as customized designs or prototypes is often not economical, and the fabrication of complex parts is very difficult due to the limited capabilities of conventional forming techniques and high tool wear.[3] There are also problems when it comes to the development of new ceramic products as design changes can only be implemented and realized in a laborious and time-consuming manner. These restrictions illustrate the need for AM technologies in the ceramic industry as it can be the remedy for these constraints.

The main limitations for widespread use of AM techniques for the production of ceramic parts were the achievable mechanical properties due to a significant discrepancy compared to conventionally produced ceramic parts. The current approaches to realize AM of ceramics can be divided into two categories, direct and indirect fabrication techniques.

Direct techniques immediately give the sintered ceramic parts without the need for thermal postprocessing. These are powder-based processes where the individual particles are connected using thermal energy input by means of a laser. Due to the generated temperature in the areas where the laser interacts with the powder, the particles melt together and the associated techniques are referred to as selective laser sintering (SLS)[4,5] or selective laser melting (SLM).[6] Problems associated with this approach are internal stresses that are induced by temperature gradients or the very rough surfaces that are obtained.[7]

Indirect AM methods require a subsequent second process step to obtain the sintered ceramic bodies. This includes all disciplines where the shaping of the objects involves a combination of the ceramic powder and an organic binder. This can mean that the feedstock already includes the binder as it is the case for laminated object manufacturing (LOM),[8,9] extrusion-based techniques such as robocasting and fused deposition modeling (FDM)[10] or methods relying on the concept of lithography like stereolithography[11,12] and digital light processing (DLP).[13] Inkjet-based techniques can either use an ink which already comprises the ceramic powder together with the binder (direct inkjet printing)[14,15] or they can use the binder alone and eject it onto a bed of ceramic particles.[16,17] In addition, there are also so-called indirect SLS methods where binder is present in the feedstock.[18] All these approaches result in the initial formation of a green part consisting of the ceramic particles and the organic binder. Upon thermal treatment of the green part, the organic components are removed and the inorganic particles are sintered to the ceramic body. This processing route is also in analogy to conventional ceramic forming where the pressed, extruded or molded green part also has to be debinded and sintered. From the group of binder-based methods, the techniques based

*mschwentenwein@lithoz.com

on lithography provide the best resolution;[2] thus, these methods have the potential to open new possibilities for the fabrication of ceramic objects, especially regarding intricate geometries, complex shapes and fine details.

Lithography-based techniques rely on the principle of photopolymerization where a liquid formulation is cured by selective space-resolved exposure to light. The initiation of the photopolymerization reaction is preceded by the excitation of the photoinitiator by absorption of light. In the excited state, the photoinitiator can either undergo a unimolecular homolytic bond cleavage to form radicals (type I photoinitiators) or react with a second molecule to give the free radicals (type II photoinitiators).[19] These radicals then start the photopolymerization process where the low molecular monomers are consumed to give long polymer chains or a polymer network causing the initially liquid formulation to solidify.

From the very beginning, lithography-based techniques played a crucial role in AM of 3D objects. The first commercial apparatus employing the AM principle was based on the concept of photopolymerization,[20] and the application of parts built using this approach ranges from technical purposes to medical use. Using lithographical techniques to fabricate 3D parts requires a photocurable feedstock; thus, the objects produced using this approach are usually made of photopolymers. However, recently, this technology has also been applied to fabricate metallic or ceramic parts.[21] Especially for ceramics materials, where AM processes had not been established so far, this methodology represents an intriguing opportunity.

Experimental

The photocurable suspension used to fabricate the alumina parts was LithaLox HP 500, a photocurable ceramic suspension that has been developed and commercialized by Lithoz. LithaLox HP 500 comprises high-purity alumina powder which is dispersed in a light-sensitive organic matrix that consists of photoinitiator, monomers based on (meth)acrylate chemistry and additives.

The 3D parts were produced on a CeraFab 7500, a lithography-based manufacturing system that has been developed and commercialized by Lithoz. The system was especially designed for the processing of highly viscous materials such as ceramic suspensions. One of the centerpieces of this system is the light engine which is based on light-emitting diodes (LEDs) and a digital micromirror device (DMD) with a resolution of 1920 × 1080 pixels. The individual mirrors of this DMD chip can be tilted causing the pixels to be turned on or off individually according to the contour of the cross section that is to be projected. Another crucial component is the dedicated projection optics. Using this optics, the individual pixels are projected with a lateral dimension of 40 × 40 μm onto the bottom of the vat. This results in a building envelope of 76.8 mm × 43.2 mm in *x*- and *y*-direction, and the uniformity of light intensity throughout this area was measured to deviate only very little at the center and the corners. The intensity in the corners was measured to be 98.4 % of the intensity in the center of the building envelope. Figure 1 shows a schematic drawing of the working chamber of the CeraFab 7500.

The data format used by the CeraFab 7500 is standard tessellation language (STL). As the underlying principle of this technology is shaping using a photocurable organic matrix, the initially produced parts are composites that require subsequent thermal treatment for debinding and sintering. Thus, the geometrical dimensions of all STL files produced by this method were scaled by a factor of 1.245 to compensate for the shrinkage upon sintering.

The quality and precision of the fabricated parts is also highly dependent on the applied processing parameters during the lithographic shaping of the parts. The LCM process provides the opportunity of defining

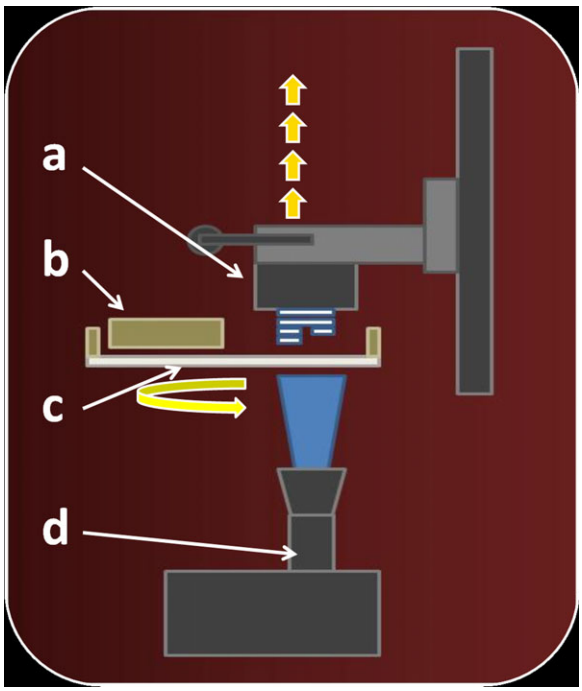

Fig. 1. Schematic drawing of the LCM process: (a) building platform; (b) wiper blade; (c) vat; (d) light engine.

numerous parameters to enable the processability of different compounds that vary either in the composition of the photocurable matrix or in the chemical nature or properties of the inorganic particles. Variations of the material will have consequences on the photoreactivity and the rheological properties of the dispersion and thus influence the processability.

Crucial parameters for the shaping process include the thickness of the layers and intensity of the light engine as well as the exposure time per layer. For this study, all parts tested or discussed within this work were fabricated using a layer thickness of 25 μm using a radiant exposure of 130 mJ/cm^2 to cure the individual layers. The radiant exposure was measured using a laser power meter (FieldMaxII-TO, Coherent, Wilsonville, OR).

The fabrication of each individual layer starts with a rotation of the vat to apply fresh slurry of a defined thickness over the building envelope. The thickness of this film is adjusted by the distance between the wiper blade and the vat bottom and is typically between 200 and 400 μm. Then, the building platform is lowered into the dispersion to a distance of 25 μm to the vat bottom. This distance has previously been set in the processing parameters and determines the thickness of each layer in the green state. When the building platform is in the right position, the space-resolved exposure of the material takes place. For this purpose, an image corresponding to the cross section of the current layer is projected onto the transparent vat bottom. Thus, photopolymerization is induced where this light interacts with the suspension and causes the slurry to solidify in this area. Subsequent to this step, the vat tilts down to separate the cured layer from the vat bottom and the building platform moves upwards out of the suspension. After this, the whole sequence is repeated again beginning with the rotation of the vat.

The rheological measurements were conducted on a rheometer (MCR 301, Anton Paar, Graz, Austria) at a temperature of 20°C and shear rates between 5 and 200/s.

Thermogravimetric analysis (TGA; TGA 2050; TA-Instruments, New Castle, DE) was performed using cylindrical samples with approximately 6 mm in diameter and 6 mm in height. The samples were heated from room temperature to 600°C at a rate of 2 K/min under ambient atmosphere.

Differential scanning calorimetry (DSC; Q2000; TA-Instruments, New Castle, DE) was performed using approximately 14 mg of the sample and heating it from room temperature to 500°C at a rate of 2 K/min.

Debinding and sintering were carried out sequentially in 2 separate furnaces, a debinding furnace (LT 5/11/HA/P330, Nabertherm, Lilienthal, Germany) for debinding as well as presintering to 900°C and a sintering aggregate (LHT 04/17, Nabertherm, Lilienthal, Germany). The sintering of the parts produced by means of LCM was done as for conventionally fabricated alumina ceramics using a heating rate of 0.8 K/min from 1150°C to 1600°C and a rate of −0.8 K/min back to 1200°C after a dwelling time of 2 h.

The characterization of the parts regarding their density was accomplished according to the Archimedean principle using a scale equipped with a density determination kit (SI-234A, Denver Instrument, Bohemia, NY).

The mechanical characterization was performed by four-point bending (4PB) tests according to DIN EN 843-1. The dimensions of the specimens were 2 × 2.5 × 30 mm, and the number of samples was 30. The tests were carried out using a universal mechanical testing machine (Z010; Zwick Roell, Ulm, Germany). Surface roughness of the sintered parts was assessed according to ISO 4287:1997 using a portable surface roughness tester (Surftest SJ-400, Mitutoyo, Kawasaki, Japan). The measurements were conducted in triplicate, and the measuring distance was 4 mm in each case. All samples were measured as fired without any grinding or polishing of the surfaces.

The microstructure of the sintered alumina samples was evaluated by means of scanning electron microscopy (SEM) on three fracture surfaces of 4PB specimens. The pictures were collected on a SEM (XL 30, FEI Philips, Eindhoven, the Netherlands). Prior to the analysis, the samples were coated with a thin layer of gold by low-vacuum sputter coating to increase their electrical conductivity.

Results and Discussion

As the LCM technology relies on the continuous deposition by a wiping mechanism, the rheological properties of the used ceramic suspension play an important role for the processing. The viscosity of the ceramic suspension was determined by rheological measurements to establish the optimum processing parameters. So far, no threshold viscosity for the shaping by means of LCM has been identified and suspensions with viscosities as high as 250 Pa·s could be processed properly; nonetheless, the viscosity of the suspension has significant impact on parameters such as processing velocities and waiting times.

The alumina suspension for these studies exhibited shear-thinning behavior as can be seen from the viscosity measurement which is depicted in Fig. 2.

At shear rates between 50 and 100/s which are typical for the LCM process, the viscosity of the suspension

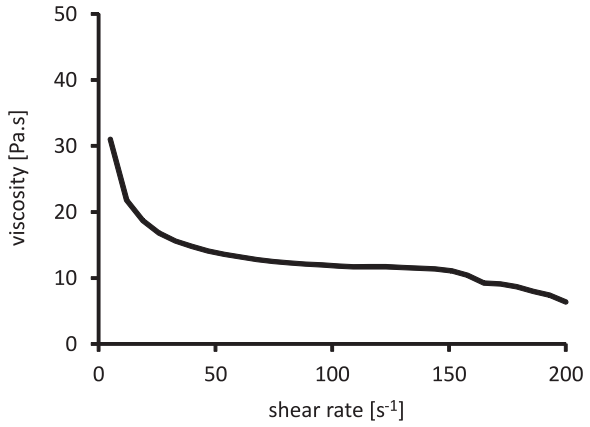

Fig. 2. Viscosity of the photocurable alumina suspension as a function of the shear rate.

was between 12 and 14 Pa·s. With such a rheological behavior, times per layer of below 30 s could be used for the shaping of the alumina parts. This setting corresponded to a uniform building speed of 3.1 mm/h over the whole building envelope.

The thermal analysis of the green parts is necessary to lay the foundation for the development of the protocol for the thermal postprocessing of the fabricated structures. These analyses involved TGA and DSC measurements.

Figure 3 shows the weight loss of the alumina green part depending on the temperature as it was measured by TGA. The figure also shows its first derivative with respect to the temperature to resolve the stages of thermal degradation. It can be seen that the thermal degradation of the organic photopolymer takes place over a broad temperature range between 150°C and 500°C. This ensures a continuous formation of decomposition products without temporary accumulation which can affect the structural integrity of the parts. However, there are two domains where the decomposition rates are higher as can be seen from the peaks of the derivative curve depicting the weight loss. This shows that at these temperature regimes, the majority of the binder is decomposed. To take this into account, the heating rates of the debinding cycle were reduced in these two domains and hold points were introduced at the onset of the decomposition peaks at 140°C and 250°C, respectively.

The DSC curve for the alumina green part is depicted in Fig. 4. The two dominating exothermic signals can be attributed to the decomposition of noncovalently bond ingredients at temperatures slightly below 200°C and to the thermal decomposition of the cross-linked photopolymer network at temperatures around 300°C to 350°C. This is also in good correspondence to the findings from the TGA analysis where also two main regimes for the weight loss of the samples are discernible. The orientation of the peaks corresponds to exothermic processes, indicating that the debinding of the green parts is realized only by the decomposition of the binder components, which is in contrast to conventionally processed alumina green parts. In green parts produced by LCM, there is a 3D cross-linked polymer network present, while in powder injection molding or pressing, only linear polymer chains are used that can also be extracted or molten out. However, in the case of a polymer network, the binder can only be removed pyrolytically.

The density measurements using the Archimedes' method gave measured values of 3.957 g/cm³ for the alumina samples. This result corresponded to 99.3 % of the theoretical density (T.D.) of alumina and showed the excellent densification for parts produced using the LCM method.

The strength of the sintered alumina specimens was determined by 4PB testing. All alumina specimens were fabricated in a an orientation that the subsequent

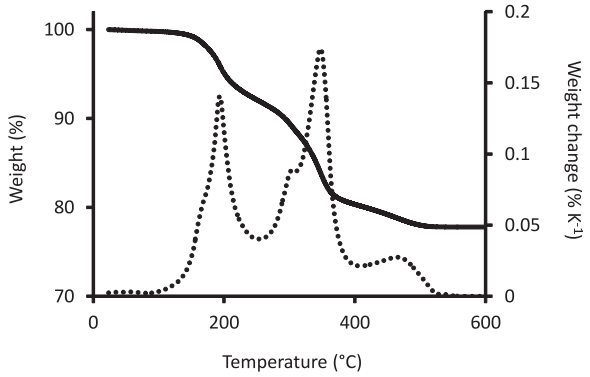

Fig. 3. TGA measurement of the alumina green part: weight (solid line) and weight change (dotted line).

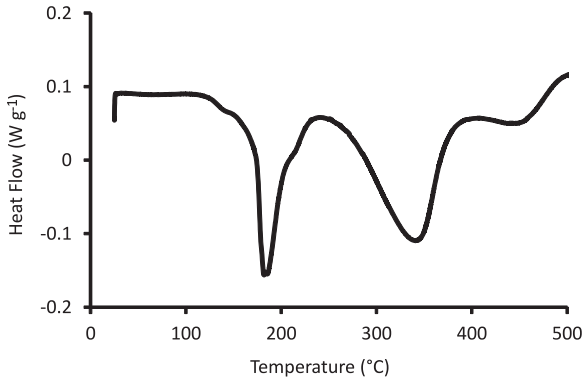

Fig. 4. DSC measurement of the alumina green part.

bending test was applying load in the direction along the layer boundaries as it is schematically illustrated in Fig. 5. Due to the layer-by-layer structure of the parts, this direction was expected to be the weakest possible. The mechanical tests gave a 4PB strength of 427 MPa and an associated Weibull modulus of 11.2. This is in good accordance with values found in the literature where a 4PB strength between 300 and 580 MPa with an accompanying Weibull modulus of 10 to 15 is mentioned for alumina.[22]

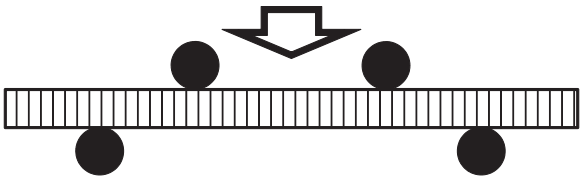

Fig. 5. Schematic set-up for 4PB testing to clarify the orientation of the individual layers.

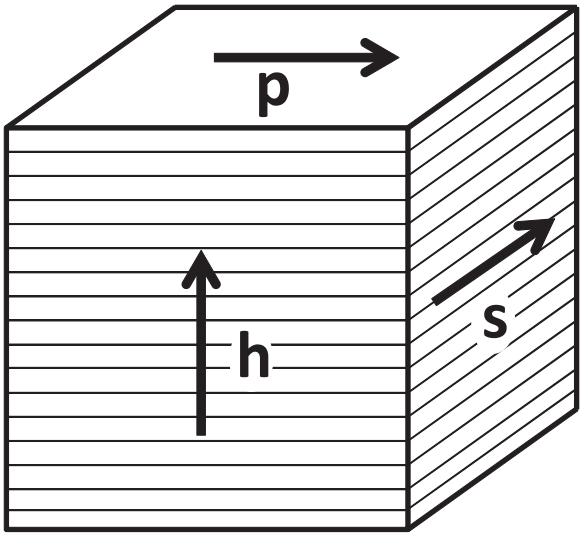

Fig. 6. Schematic drawing for roughness measurements to clarify the orientation of the individual layers.

The surface roughness measurements led to slightly varying results depending on the measuring direction and the orientation of the surface as it is schematically illustrated in Fig. 6. The roughness average R_a was 0.84 μm along the layer boundaries (s) and 1.08 μm perpendicular to the individual layers in shaping direction (h). As expected, the best surface quality was measured in the plane of an individual layer (p) with a R_a value of only 0.36 μm. These different values are caused by the layer-by-layer build up of objects produced by means of LCM. While the individual layers merge together upon sintering, on the outside of the fabricated objects remain grooves from the layer boundaries at a microscopic level. Nonetheless, the surface roughness is comparable to injection molded parts and significantly better by means of other nonlithographic based AM techniques such as laser sintering, where significantly higher Ra values around 20 μm are reported.[23]

This general evaluation showed that the properties of parts produced by LCM are very similar to those of conventionally formed parts. Thus, these objects can be used in the same technological applications as their counterparts that are produced by traditional means. This can lead to new possibilities with respect to the fabrication of small-scale series, even down to lot sizes of 1. Moreover, the geometrical freedom arising from the layer-by-layer shaping principle enabled the fabrication of highly complex and intricate architectures as it is shown in Fig. 7. This figure shows examples for typical applications of AM technologies, production of small-scale series as for the gear wheels, individual prototypes like the depicted turbine blade or highly complex geometries as in the case of the cellular cube. In the case of the cellular structure, the strut thickness goes down to 200 μm. Minimum feature sizes for this method were

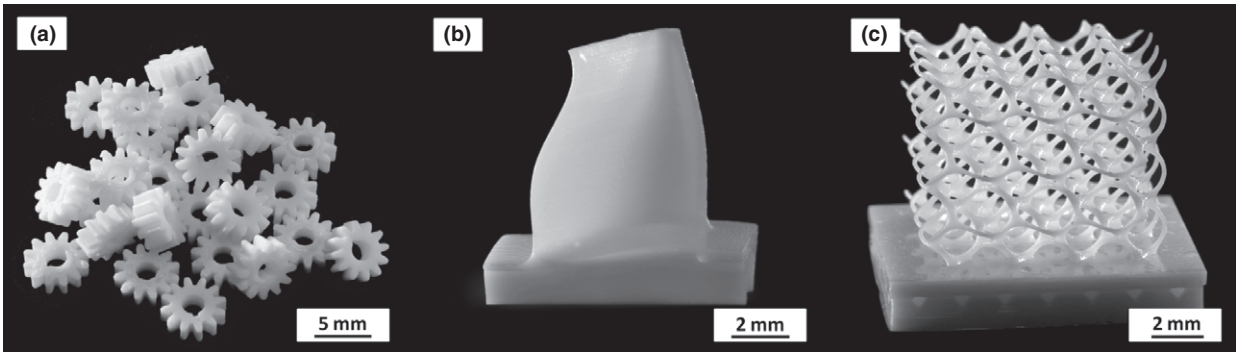

Fig. 7. Sintered alumina parts fabricated using the LCM technique: (a) gear wheels; (b) a turbine blade; and (c) a cellular cube.

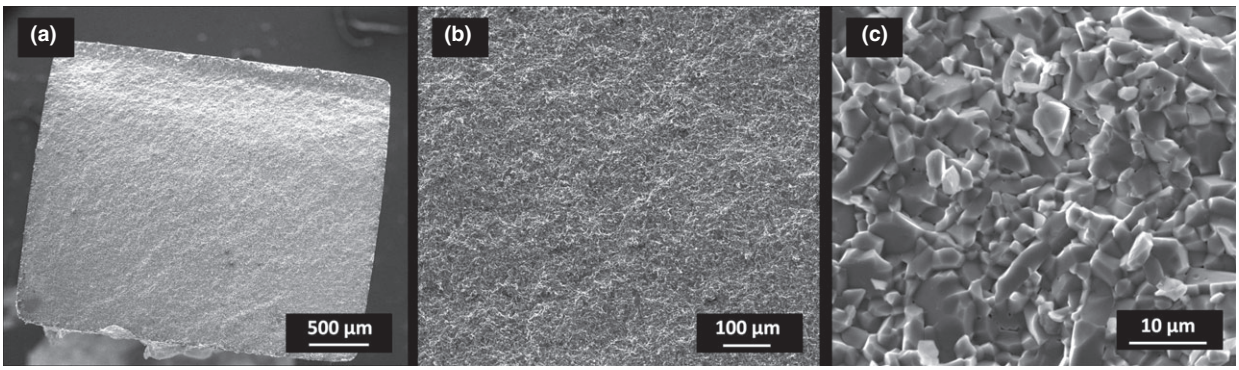

Fig. 8. SEM micrographs of the 4PB fracture surfaces of the sintered alumina specimens in different magnifications.

approximately 125 µm for walls or struts and 200 µm for defined pores or channels.

Fracture surfaces of three of the 4PB specimens were analyzed under the scanning electron microscope (SEM) to get information on the microstructure of the parts. The observed fracture pattern and microstructure were very similar among the tested samples, and Fig. 8 shows exemplary fracture surfaces of the alumina test parts at different magnifications.

An important finding was that the fracture surface of the specimens was oriented randomly without any visible preferential direction along the boundaries between adjacent layers. Thus, it can be concluded that these interlaminar regions do not act as predetermined breaking points.

It can be seen that a dense and uniform microstructure could be achieved as it was already indicated by the density measurements. The average grain size was found to be 3.05 µm with a standard deviation of 0.29 µm. As for conventional ceramics, further structural characteristics such as the crystallite sizes and their distribution are governed by other factors such as the presence of dopants or the sintering protocol and not limited by the shaping method.

Conclusions

The introduction and commercialization of a new AM technique for ceramic parts by the photolithographic LCM process enabled the fabrication of dense and accurate structures of high complexity. The parts manufactured using the CeraFab 7500 system exhibited mechanical properties equivalent to ceramic materials structured by conventional means. Using photocurable ceramic suspensions in combination with DLP technology enabled fast and reproducible fabrication of complex alumina structures directly from CAD drawings. With densities above 99.3 % T.D. and 4PB strength of 427 MPa, the achievable mechanical properties are comparable to those of conventional alumina ceramics. Thus, this methodology can be employed to produce technical ceramic products and is especially suitable for small lot sizes or customized parts. In addition, this technology provides new opportunities to realize very complex geometries and delicate features, making this approach a capable complement to conventional processing techniques for the fabrication of ceramic parts.

Acknowledgments

The authors would like to thank the Vienna University of Technology for the assistance for the thermomechanical characterization experiments. Also the financial support of this work by the Austrian Research Promotion Agency (FFG) under the project number 834367 is kindly acknowledged.

References

1. X. Tian, D. Li, and J. G. Heinrich, "Net-Shaping of Ceramic Components by Using Rapid Prototyping Technologies"; in Adv. Ceram. - Synth. Charact. Process. Specif. Appl. 2011.
2. R. Knitter, and W. Bauer, *Sadhana*, 28 [1–2] 307–318 (2003).
3. W. Y. Yeong, C. Y. Yap, M. Mapar, and C. K. Chua, "State-of-the-art review on selective laser melting"; pp. 65–70 in High Value Manuf. Adv. Res. Virtual Rapid Prototyp. Proc. 6th Int. Conf. Adv. Res. Virtual Rapid Prototyp., Leiria, Portugal, October 1-5, 2013.
4. P. Bertrand, F. Bayle, C. Combe, P. Goeuriot, and I. Smurov, *Appl. Surf. Sci.*, 254 [4] 989–992 (2007).
5. H. Exner, *et al.*, *Virtual Phys. Prototyp.*, 3 [1] 3–11 (2008).
6. Y.-C. Hagedorn, J. Wilkes, W. Meiners, K. Wissenbach, and R. Poprawe, *Phys. Procedia*, 5 Part B 587–594 (2010).
7. W. Kollenberg, *Technische Keramik (Technical Ceramics)*, 2nd edition, Vulkan, Essen, Germany, 2009.
8. I. Götschel, B. Gutbrod, N. Travitzky, A. Roosen, and P. Greil, *Adv. Appl. Ceram.*, 112 [6] 358–365 (2013).

9. H. Windsheimer, N. Travitzky, A. Hofenauer, and P. Greil, *Adv. Mater.*, 19 [24] 4515–4519 (2007).
10. L. Novakova-Marcincinova, J. Novak-Marcincin, J. Barna, and J. Torok, "Special materials used in FDM rapid prototyping technology application"; pp. 73–76 in 2012 IEEE 16th Int. Conf. Intell. Eng. Syst. INES. 2012.
11. T. Chartier, A. Badev, Y. Abouliatim, P. Lebaudy, and L. Lecamp, *J. Eur. Ceram. Soc.*, 32 [8] 1625–1634 (2012).
12. A. Badev, *et al.*, *J. Photochem. Photobiol. Chem.*, 222 [1] 117–122 (2011).
13. R. Felzmann, *et al.*, *Adv. Eng. Mater.*, 14 [12] 1052–1058 (2012).
14. J. Ebert, *et al.*, *J. Dent. Res.*, 88 [7] 673–676 (2009).
15. J. Wang, and L. L. Shaw, *J. Am. Ceram. Soc.*, 89 [10] 3285–3289 (2006).
16. B. Leukers, *et al.*, *J. Mater. Sci. Mater. Med.*, 16 [12] 1121–1124 (2005).
17. M. Mott, and J. R. G. Evans, *J. Am. Ceram. Soc.*, 84 [2] 307–313 (2001).
18. K. Shahzad, J. Deckers, J.-P. Kruth, and J. Vleugels, *J. Mater. Process. Technol.*, 213 [9] 1484–1494 (2013).
19. J. P. Fouassier, and J. Lalevée, *Photoinitiators for Polymer Synthesis: Scope, Reactivity, and Efficiency.* John Wiley & Sons, Weinheim, 2013.
20. C. W. Hull, U.S. Patent 4575330 A, 1986.
21. A. Clarinval, R. Carrus, T. Dormal, and Q. Soyeur, *Adv. Res. Virtual Rapid Prototyp.*, 41 5–418 (2007).
22. Informationszentrum Technische Keramik, Brevier Technische Keramik (Brevier Technical Ceramics), 4th edition, p. 270, Fahner Verlag, Lauf, Germany, 2003.
23. J. Deckers, J.-P. Kruth, L. Cardon, K. Shahzad, and J. Vleugels, *Stroj. Vestn.-J. Mech. Eng.*, 59 [11] 646–661 (2013).